

# Lawrence Berkeley National Laboratory

## Lawrence Berkeley National Laboratory

### Title

UXO detection and identification based on intrinsic target polarizabilities: A case history

### Permalink

<https://escholarship.org/uc/item/5m5028m7>

### Author

Gasperikova, E.

### Publication Date

2009-02-26

# **UXO DETECTION AND IDENTIFICATION BASED ON INTRINSIC TARGET POLARIZABILITIES - A CASE HISTORY**

Erika Gasperikova, J. Torquil Smith, H. Frank Morrison, Alex Becker, and Karl Kappler

Lawrence Berkeley National Laboratory

One Cyclotron Road, MS: 90R1116, Berkeley, CA 94720

egasperikova@lbl.gov

UXO detection and identification

## **ABSTRACT**

Electromagnetic induction data parameterized in time dependent object intrinsic polarizabilities allow discrimination of unexploded ordnance (UXO) from false targets (scrap metal). Data from a cart-mounted system designed for discrimination of UXO with 20 mm to 155 mm diameters are used. Discrimination of UXO from irregular scrap metal is based on the principal dipole polarizabilities of a target. A near-intact UXO displays a single major polarizability coincident with the long axis of the object and two equal smaller transverse polarizabilities, whereas metal scraps have distinct polarizability signatures that rarely mimic those of elongated symmetric bodies. Based on a training data set of known

targets, object identification was made by estimating the probability that an object is a single UXO. Our test survey took place on a military base where both 4.2” mortar shells and scrap metal were present. The results show that we detected and discriminated correctly all 4.2” mortars, and in that process we added 7%, and 17%, respectively, of dry holes (digging scrap) to the total number of excavations in two different survey modes. We also demonstrated a mode of operation that might be more cost effective than the current practice.

## **INTRODUCTION**

Unexploded ordnance (UXO), partly resulting from the high rate of failure among munitions from more than 60 years ago, present serious problems in Europe, Asia, and the United States. In Europe and Asia, World War I and II UXO still turn up at construction sites, in backyard gardens, on beaches, wildlife preserves, and former military training sites. In the U.S., a considerable amount of UXO was generated at former military bases, as a result of decades of training, exercises, and testing of weapons systems. Such UXO contamination prevents civilian land use, threatens public safety, and causes significant environmental concern. In light of this problem, there has been considerable interest shown by federal, state, and local authorities in UXO remediation at former U.S. Department of Defense sites. The ultimate goal of UXO remediation is to permit safe public use of contaminated lands. A Defense Science Board Task Force Report from 2003 lists some 1,400 sites, comprising approximately 10 million acres, that potentially contain UXO. This report also noted that 75% of the total cost of a current

response action is spent on digging scrap. Reducing the number of scrap items dug per munitions item from 100 to 10 could reduce total response action costs by as much as two-thirds. The Task Force assessment was that much of this wasteful digging can be eliminated by the use of more advanced instruments that exploit modern digital processing and advanced multi-mode sensors to achieve an improved level of discrimination of scrap from UXO.

The search for UXO is a two-step process. The object must first be detected and its location determined; then the parameters of the object must be defined. The first step is now accomplished with a variety of magnetometer and active electromagnetic (AEM) systems. These AEM systems operate in the transient or frequency domain mode, and until recently used a single transmitter and up to three receivers (i.e., McNeill and Bosnar, 1996; Won et al., 1997). The second step involves generation of incident fields that induce magnetization and current flow in different directions within the object. The magnetic dipole moments induced in the body, normalized by the inducing field, are known as the polarizabilities of the object. In fact, equivalent dipole approximations have been used in geophysics as well as other fields for a long time. In recent applications, they have been used to model secondary magnetic fields arising from currents induced in isolated conductive, and possibly magnetic, bodies for discrimination of UXO from scrap metals (e.g., see Baum, 1999; Bell et al., 2001; Khadr et al., 1998; and Pasion and Oldenburg, 2001). In these examples, the induced dipoles were taken to be linearly proportional to the inducing magnetic fields at the body centers. Smith and Morrison (2004) give a particularly clear treatment of the problem of estimating object location and polarizability matrices, restraining the non-linearity of the problem to three dimensional

space, and solving the rest of the problem using linear methods. The secondary fields related to these induced polarizabilities, as a function of frequency or time, are the measured quantities. These polarizabilities, and their variations with either time or frequency, are the only fundamental object parameters that can be recovered from the inductive excitation of a finite body in the ground, if a dipolar representation is assumed.

For regular bodies of revolution the induced moments are aligned with the symmetry axes of the object, and for a uniform inducing field, do not change direction with time or frequency. However, for an irregular object such as twisted scrap metal, the moment directions do change with time or frequency.

Previous AEM systems have had only one transmitter, hence illuminating the object in different directions required multiple measurements. This was not only time consuming, but also tedious. At each anomaly location, a template with predefined system locations was laid on the ground, and data were acquired with the system positioned at each of these locations. In recent years, multicomponent AEM systems have been developed with the potential not only of detecting UXO, but also of determining its depth, size, shape, and metal content, even in the presence of metallic clutter and a heterogeneous background. This capability has the potential to significantly increase detection rates, lower false alarm rates, and, more importantly, enhance our ability to discriminate between intact UXO and scrap metal.

In this paper we demonstrate the use of a multicomponent AEM system, both for detection and for target characterization. Using three orthogonal transmitters and multiple receivers, object location and characterization can be done using data from a single site. Our objective was to evaluate the discrimination capability of this approach. The field

site was chosen because of the known mixture of UXO and scrap metal. Furthermore, all detected anomalies were excavated, and ground truth was available for verification of the geophysical results. As a part of new decision-making processes, a new definition of a Receiver Operating Curve (ROC) has been proposed by the Institute for Defense Analyses (IDA) (Cazares et al., 2008) and it is used to present our results.

A comprehensive summary and comparison of existing systems and their performance at various test sites was published in two reports, Geophysical Prove-Outs for Munitions Response Projects by ITRC (2004), and Survey of Munitions Response Technologies by ESTCP, ITRC and SERDP (2006). In recent years, significant progress has been made in discrimination technology, which includes both instrumentation and data processing and discrimination algorithms (e.g., Gasperikova et al., 2006 & 2007; Huang et al., 2007; Pasion et al., 2007; Snyder and George, 2005; Wright et al., 2007). However, acceptance of discrimination technologies by regulators requires the demonstration of system capabilities as well as the entire decision-making processes at real UXO sites, under real operating conditions. The first such effort was a recent discrimination study at a former military training range organized by the Environmental Security Technology Certification Program (ESTCP).

## **METHODS AND INSTRUMENTATION**

### **Instrumentation**

We found in our design process that AEM systems scale roughly with depth of burial and target size. Thus the dimensions of the transmitter control the field strength at

depth and the spacing of receivers controls the accuracy of depth estimates. Smith and Morrison (2005) showed that a minimum of 13 independent transmitter-receiver data points are necessary to unambiguously determine the target parameters. Given the possibility of an arbitrary number of receivers, the overall system dimensions are set by the size of the transmitter loop and the practicality of moving this loop over the ground. Our prototype instrument BUD (which stands for the Berkeley UXO Discriminator), shown in Figure 1a is a time-domain AEM system designed to detect UXO in the 20 mm to 155 mm size range for depths between 0 and 1.5 m, and to characterize them in a depth range from 0 to 1.1 m. The system was described by Smith et al. (2007), and results from a local test site and the Yuma Proving Ground have been presented by Gasperikova et al. (2006, 2007). The system is made up of three orthogonal transmitters and eight pairs of differenced receivers. The footprint of the system is  $1 \times 1$  m. The transmitter-receiver assembly and the acquisition box, along with the battery power and state-of-the-art real time kinematic (RTK) global positioning system (GPS) receiver are mounted on a small cart to assure system mobility.

We use a  $340 \mu\text{s}$  half-sine pulse current waveform, repeated every  $1852 \mu\text{s}$  with alternating polarity. A series of nine pulses is fed to each of the three transmitters in turn and stacked over 20 such sequences, cancelling harmonics of 60 Hz. The receivers are critically damped dB/dt induction coils with a nominal resonance frequency of 20 kHz, and are designed to minimize the transient response of the primary field pulse. The eight receiver coils (Figure 1b) are placed horizontally along the two diagonals of both the upper and lower planes of the two horizontal transmitter loops. The receiver coils are paired along symmetry lines through the center of the system, so that each pair sees

identical fields during the on-time of the current pulses in the transmitter coils. They are wired in opposition to produce zero output during the on-time of the pulses in the three orthogonal transmitters. This configuration dramatically reduces noise in the measurements by canceling background electromagnetic fields (these fields are uniform over the scale of the receiver array and are consequently nulled by the differencing operation) and by canceling noise contributed by the movement of the receivers in the Earth's magnetic field, thus greatly enhancing receiver sensitivity to gradients of the target response. The target transient is recovered in a 140 to 1400  $\mu\text{s}$  window.

### **UXO Identification Using Polarizabilities Curves**

The induced moment of the target depends on the strength of the transmitted inducing field. That moment, when normalized by the inducing field is the target polarizability. The secondary fields measured as a function of time, are related to the induced polarizabilities. The polarizabilities and their variation with time are the only fundamental object parameters that can be recovered from the inductive excitation of a finite body in the ground if a dipolar representation is assumed. Smith and Morrison (2004) demonstrated that a satisfactory classification scheme is one that determines the principal dipole polarizabilities of a target. Nearly intact UXO displays a single major polarizability coincident with the long axis of the object, and two equal smaller transverse polarizabilities, whereas scrap metal exhibits three distinct principal polarizabilities. Measurement results shown in Figures 2 and 3 illustrate the ability of the multi-component AEM system to discriminate between UXO (Figure 2) and scrap metal (Figure 3). Both figures show the estimated principal polarizabilities plotted as a function



of time, with the corresponding object images at the bottom of the illustration. As predicted, UXO targets have a single major polarizability coincident with the long axis of the object and two equal smaller transverse polarizabilities (cf. Figure 2), whereas the scrap metal exhibits three distinct principal polarizabilities (cf. Figure 3). These results clearly show that the intrinsic polarizabilities of the target can be resolved, and that there are very clear distinctions between symmetric intact UXO and irregular scrap metal. Moreover, intact UXO have unique responses that allow for discrimination between the various UXO objects. This last characteristic was not used at this particular site but is essential at any site where a variety of munitions is present.

When the target is far enough from the system such that the uniform field illumination and a dipole approximation are valid, the interpreted polarizabilities are independent of object depth and orientation. For large objects close to the system however, the principal polarizability curves vary with the orientation of the object. Object orientation estimates and equivalent dipole polarizability estimates for large and shallow objects are affected by higher-order (nondipole) terms induced in objects as a result of source-field gradients along the length of the objects. For example, a vertical 0.4 m long object (for example, 4.2" mortar) directly below the system needs to be about 0.90 m deep for perturbations caused by gradients along the length of the object to be on the order of 20% of the uniform field object response. This calculation was done with an assumption that the object needs to be approximated by two dipoles, each a quarter length from the object edge, rather than by a single dipole in the center of the object. For horizontal objects, the effect of gradients across the objects' diameter is much smaller. For example, 0.4 m long object needs to be only 0.20 m below the system to be correctly located and identified.

A polarizability index (in  $m^3$ ), an average value of the product of time (in seconds) and polarizability value (in  $m^3/s$ ) over the 35 sample times logarithmically spaced from 140 to 1400  $\mu s$ , and three polarizabilities, can be calculated from the response of any object. We used this polarizability index to decide when the object is in a uniform source field. Based on UXO from the Yuma Proving Ground Calibration Grid together with the object lengths, objects with the polarizability index smaller than 600  $cm^3$  and deeper than 1.8 m below the system (or smaller than 200  $cm^3$  and deeper than 1.35 m, or smaller than 80  $cm^3$  and deeper than 0.90 m, or smaller than 9  $cm^3$  and deeper than 0.20 m below the system) are sufficiently deep that the effects of vertical source field gradients should be less than 15%. To assure proper object identification and UXO/scrap discrimination, in the case of large and shallow objects, we took measurements at five sites spaced 0.5 m along a line traversing the object. The data from the site at which the line from the estimated object center to the lower receiver plane center was closest to being perpendicular to the orientation of the objects' interpreted axis of greatest polarizability were used for discrimination.

In the case where no training data are available, our object identification program matches the measured equivalent dipole polarizabilities to a database of previous measurements of equivalent dipole polarizabilities of known objects ('exhaustive search'), and identifies a candidate object as the object(s) corresponding to the closest matching curves from the database. This is done by minimizing a robust loss function of the normalized absolute differences (residuals) between the measured values and those in the database, weighted inversely by estimated uncertainty in polarizabilities.

## UXO/Scrap Discrimination Using Training Data

For the UXO/scrap discrimination, we used a training data set that contained the principal polarizability responses of 100 objects - 45 mortars, 13 half-rounds, and 42 pieces of scrap metal (37 objects were from the geophysical prove out area (GPO), 27 objects from the cued area, and 36 objects from the survey area). A description of the survey and cued areas is given in “Field Survey and Results” section. This was considered to be a realistic training data set that in addition to the responses from the GPO area would include also responses of 10-15% of the objects that require discrimination. Two-thirds of the training data were randomly selected for direct use in training, and one third was reserved for later calibration.

The data time interval was subdivided logarithmically into a number ( $n_{\text{div}}$ ) of subintervals. The product of each principal polarizability and its sample time was averaged over each of these intervals. Since there are three principal polarizabilities, this resulted in  $n_{\text{feat}} = 3n_{\text{div}}$  reduced data, henceforth called “features.” We used an additional feature, the logarithm of the vector magnitude of the above  $3n_{\text{div}}$  features (in  $\text{m}^3$ ), which increased the total number of features  $n_{\text{feat}}$  to  $3n_{\text{div}}+1$ . When this feature is added, the partial vector of  $3n_{\text{div}}$  features is rescaled to have unit magnitude. The number of subdivisions  $n_{\text{div}}$  was chosen using cross validation. In cross validation, results from a subset of training data was used to predict something about the remaining training data. This was done many times (“repeats”), excluding a different set of training data each time, and then a choice was made based on what gave the best predictions averaged over the many repeats. For the UXO versus scrap discrimination problem, the average cross-validated estimated probability of UXO being scrap ranged from 0.0892, when the

number of subintervals ( $n_{\text{div}}$ ) was 3 (10 features), to 0.0336 for  $n_{\text{div}} = 6$  (19 features), which further decreased to 0.0222 when responses reserved for calibration were included. As a result, we used  $n_{\text{div}} = 6$  in our discrimination.

For the training data (UXO or scrap) with  $n_{\text{div}} = 6$ , the feature vector contained 19 features—median features at six different times for each of the three principal polarizability curves, and the median  $\log_e(\text{magnitude})$ . Each of the features had its median and median absolute deviation (MAD) computed separately for UXO and scrap training data. There was a greater spread in the three median principal polarizabilities of the scrap responses than of the UXO responses, and the scrap median log magnitude was slightly smaller. The MADs showed greater variability in the scrap features than in the UXO ones, reflecting greater variability in ratios of scrap principal polarizabilities than in those of UXO.

For convenience, features were differenced with median values (for UXO or scrap) and normalized by feature MADs (for UXO or scrap), separately for consideration as UXO or scrap, and denoted by  $\mathbf{v}_i^{(\text{uxo})}$  or  $\mathbf{v}_i^{(\text{scrap})}$  for the two normalizations, respectively. Training data from UXO and scrap classes were used to form trimmed-feature covariance matrices for the two classes separately:

$$C^{(\text{class})} = \frac{1}{n^{(\text{class})}} \left[ \sum_{i \text{ in class, } |\mathbf{v}_i^{(\text{class})}| \leq \text{median}} \mathbf{v}_i^{(\text{class})} (\mathbf{v}_i^{(\text{class})})^t + \sum_{i \text{ in class, } |\mathbf{v}_i^{(\text{class})}| > \text{median}} \text{median}^2 \frac{\mathbf{v}_i^{(\text{class})} (\mathbf{v}_i^{(\text{class})})^t}{|\mathbf{v}_i^{(\text{class})}|^2} \right], \quad (1)$$

where (class) is either (uxo) or (scrap),  $t$  denotes transpose, and  $n^{(\text{class})}$  is the number of (class) responses. In the second sum, the contribution of large magnitude feature vectors are downweighted. A feature vector  $\mathbf{v}_i^{(\text{class})}$  probability density function is estimated empirically as proportional to

$$f^{(\text{class})}(v_j^{(\text{class})}) = \frac{1}{K \sum_{i \text{ in class}} \left[ 1 + \gamma(v_j^{(\text{class})} - v_i^{(\text{class})})^t (C^{(\text{class})})^{-1} (v_j^{(\text{class})} - v_i^{(\text{class})}) (n^{(\text{class})})^{2/n_{\text{feat}}} \right]^{(n_{\text{feat}} + p_{\text{extra}})/2}} \quad (2)$$

with

$$1/K = (n^{(\text{class})})^{(1+n_{\text{feat}})/n_{\text{feat}}} (\det(C^{(\text{class})}))^{1/2} \quad \text{and} \quad (3a)$$

$$\gamma = 0.2986/(n_{\text{feat}} + p_{\text{extra}}) \quad (3b)$$

Equation (2) is a generalization of a Cauchy distribution. As  $p_{\text{extra}}$  approaches infinity the distribution approaches a Gaussian distribution. With parameter  $p_{\text{extra}} = 3$  the outer exponent has the smallest half-integer value for which distribution has a finite variance. This value was used, allowing for very heavy tailed distributions. This was slightly conservative for the mortar responses, for which  $p_{\text{extra}} = 9$  was the maximum likelihood value, and very conservative for the scrap responses, which approached a Gaussian distribution. Density estimate (2) could be further refined by additional blurring of the contributions of training data with large uncertainties.

Assuming equal a priori probability of being UXO or scrap, the probability of the response being caused by scrap is:

$$p^{(\text{scrap})}(v_j^{(\text{scrap})}) = \frac{f^{(\text{scrap})}(v_j^{(\text{scrap})})}{f^{(\text{uxo})}(v_j^{(\text{uxo})}) + f^{(\text{scrap})}(v_j^{(\text{scrap})})} \quad (4)$$

(Bayes' rule, e.g., Hoel et al., 1971) and the probability of the response being caused by UXO is:

$$p^{(\text{uxo})}(v_j^{(\text{uxo})}) = 1 - \frac{f^{(\text{scrap})}(v_j^{(\text{scrap})})}{f^{(\text{uxo})}(v_j^{(\text{uxo})}) + f^{(\text{scrap})}(v_j^{(\text{scrap})})} \quad (5)$$

Allowing for unequal a priori probability of a response being due to UXO or scrap, with their ratio being  $\alpha^2$ , the probability that the response is due to scrap is:

$$p^{(\text{scrap})}(\mathbf{v}_j^{(\text{scrap})}) = \frac{f^{(\text{scrap})}(\mathbf{v}_j^{(\text{scrap})})}{\alpha^2 f^{(\text{uxo})}(\mathbf{v}_j^{(\text{uxo})}) + f^{(\text{scrap})}(\mathbf{v}_j^{(\text{scrap})})} \quad (6)$$

and the probability that the response is due to UXO is

$$p^{(\text{uxo})}(\mathbf{v}_j^{(\text{uxo})}) = 1 - \frac{f^{(\text{scrap})}(\mathbf{v}_j^{(\text{scrap})})}{\alpha^2 f^{(\text{uxo})}(\mathbf{v}_j^{(\text{uxo})}) + f^{(\text{scrap})}(\mathbf{v}_j^{(\text{scrap})})} \quad (7)$$

Probabilities in Equations (6) or (7) formed the basis for the discrimination between UXO (mortar) and scrap classes.

The class feature covariance matrices  $C^{(\text{uxo})}$  and  $C^{(\text{scrap})}$ , and the densities  $f^{(\text{uxo})}$  and  $f^{(\text{scrap})}$  were computed from subsets of the training data. UXO and scrap probabilities—Equations (6) and (7)—were estimated for the remaining (excluded) training data. Estimated UXO probabilities of excluded training data were summed over many repeats. Parameter  $\alpha^2$  was adjusted (using Newton’s method), so that the summed UXO probabilities yield the true number of UXO in the training set. When the ratio of mortar training examples to scrap training examples is their true relative probability, and  $f^{(\text{uxo})}(\mathbf{v}_i^{(\text{uxo})})$  and  $f^{(\text{scrap})}(\mathbf{v}_i^{(\text{scrap})})$  are the true densities, this procedure operating on expected values, yields the correct value of  $\alpha^2$ . When the ratio of mortar training examples to scrap training examples is greater than their true relative probability, this procedure will tend to over estimate  $\alpha^2$  and the ensuing estimates of  $p^{(\text{uxo})}$ . This was done for  $n_{\text{div}}$  from 1 to 6 and the  $n_{\text{div}}$  that gave the lowest summed estimated probabilities of being scrap for the UXO in the training data set was selected. After this calibration, the algorithm was applied to the set of unknown responses, and the discrimination between UXO and scrap

classes was conducted using Equation (6) and (7). A threshold value was selected, and every response with  $p_{\text{uxo}}(v^{(\text{uxo})})$  less than the threshold  $p_o^{(\text{uxo})}$  was classified as scrap; the rest were classified as UXO (mortars).

## FIELD SURVEY AND RESULTS

At the military test site, the primary UXO targets were 4.2'' (107 mm) mortars (Figure 2) about 0.4 m long. The system detection threshold was based on the signal strength relative to levels of a background response variation. Measured signal strengths (field value) normalized by the background variation for a 4.2'' mortar as a function of depth are shown in Figure 4. The solid line indicates the response of the 4.2'' mortar in a horizontal (least favorable) orientation, and the dashed line indicates the response of the 4.2'' mortar in a vertical (most favorable) orientation. The detection threshold was set to ten, which is 50% of the value that would be measured for the 4.2'' mortar at the depth equal to 11 times the diameter of the mortar.

We demonstrated two modes of operation: (1) the simultaneous detection and characterization/discrimination, and (2) the cued mode. In the first mode, the survey area was divided into one hundred 200 m long lines oriented approximately east-west. Line spacing in the orthogonal direction (north-south) was 1 m. We conducted the survey at a speed of 0.5 m/s. The cart-mounted system was pushed along the line at a constant speed in the search mode, with data recorded and stored continuously. In principle, any object within the  $1 \times 1$  m footprint of the horizontal transmitter coil and 1.2 m in front of the system can be detected and characterized. In the search mode, the operator was alerted to

the presence of a target every time the signal level exceeded the detection threshold. The operator then stopped, and a full sequence of measurements was initiated. The three discriminating polarizability responses were recorded and visually presented on the computer screen. Then the cart again was moved at a constant speed in the search mode until the next target was detected and the discrimination process was repeated. An average daily coverage in this mode of operation was 0.5 acres ( $\sim 2000 \text{ m}^2$ ). This mode of operation has the advantage that target reacquisition is not necessary for characterization. As described earlier, for the case in which a large shallow object was found, we collected five measurements spaced 0.5 m along a line traversing the object (that is, if the object location was at 0.0, measurements were taken at 1.0 m, 0.5 m, 0.0 m, -0.5 m, and -1.0 m), so that the system moved further away from the object, and hence minimized source gradients at one or more locations. The measurement that best satisfied the criteria described earlier was used for the object characterization.

In addition to the 4.2" mortars and half-rounds shown in Figures 2 and 3, the area contained a lot of scrap metal; some representative responses are shown in Figure 5 and 6. Scrap metal ranged from pieces as small as  $4 \times 1 \times 1 \text{ cm}$ , through  $10.5 \times 10.5 \times 4 \text{ cm}$  base plates, up to  $28 \times 17 \times 0.5 \text{ cm}$  half-rounds. All the objects had distinct polarizability signatures, which allowed for a clear discrimination between the 4.2" mortars and scrap metal.

Figure 7 shows the detection map of our survey area. Colors represent measured signal strength normalized by the background variation. Since the detection threshold was set to ten (Figure 4), red and yellow colors represent the background response, while green and blue colors indicate locations of metallic objects. For the 4.2" mortar, the



polarizability index is larger than  $300 \text{ cm}^3$ . Consequently, the detection list contained every object with a response above the detection threshold or polarizability index larger than  $150 \text{ cm}^3$ . We identified 358 such locations. Some of these locations did not have the ground truth, some of the objects were a part of the training data set and some of them where multiple objects, hence the survey area discrimination set, provided to us by the IDA, contained 266 objects.

We provided discrimination results in the form of two priority dig lists. In the first one, the “stop digging” point was chosen when any object past this point had an estimated probability of 0.01% of being a 4.2” mortar, and 0.1% probability of leaving any UXO in the ground. The second priority dig list had the “stop digging” point at 90% probability of any object being a 4.2” mortar. In the first priority dig list, we indicated that 75 objects had to be dug (i.e., UXO), whereas 191 objects could be left in the ground (i.e., scrap metal). The second priority list classified 63 objects as “need to dig” and 203 objects that could be left in the ground.

The ground truth data indicated that 56 of the objects were single 4.2” mortars. Scoring results from the IDA showed that the system performed extremely well. We identified correctly all 56 4.2” mortars in both cases, and we identified scrap as 4.2” mortar 19-times (19 false positives) in the first case, and 7-times in the second case.

The ROC curve for the survey area priority dig list is shown in Figure 8a. The results are plotted with the number of false positives on the x-axis and the probability of discrimination on the y-axis. The green line shows objects that we identified as scrap, the red line indicated objects we identified as UXO. The dark blue circle represents a “stop digging” point from our interpretation, the magenta circle shows the number of false

positives if the probability would be 95%, and the cyan circle shows the number of false positives if the probability would be 100%. The gray shaded area indicated 95% confidence interval. The graph shows that the system performed extremely well: we correctly discriminated all mortars (cyan and magenta circles), and we had 19 false positives (dark blue circle), which would be only 7% of unnecessary excavations based on the total number of possible excavations.

In addition to the survey described above, we performed a cued survey over 200 objects. In this case, the system was brought to marked locations and run in the discrimination mode. The three discriminating polarizability responses were recorded and visually presented on the computer screen. Again, for large shallow objects, we collected five measurements spaced 0.5 m along a line traversing the object, and the measurement that best satisfied the criteria described earlier was used for the object characterization.

From 200 cued survey locations, 27 objects were included in the training data set, and 23 others were identified as multiple objects and therefore the IDA excluded those from the cued discrimination set. Again, we provided discrimination results for the remaining 150 objects in the form of two priority dig lists. The first one, with the “stop digging” point at which any object past this mark had an estimated probability of 0.01% of being a 4.2” mortar, and 0.1% probability of leaving any UXO in the ground. This list indicated that 90 objects could be left in the ground, and 60 objects had to be dug. The second priority dig list had the “stop digging” point at 90% probability of any object being a 4.2” mortar. In this list, only 43 objects were identified as “need to dig,” while 107 could be left safely in the ground.

The ground truth revealed that 34 of them were 4.2” mortars. Scoring results from the IDA showed that in both cases we correctly identified all 4.2” mortars. In the first, more conservative, priority dig list, we had 26 false positives—we identified scrap as UXO 26 times. In the second dig list, where the “stop digging” point was at 90% probability of any object being 4.2” mortar, we reduced false positives to 9.

The ROC curve for the cued target priority dig list is shown in Figure 8b. Again, the results are plotted with the number of false positives on the x-axis and the probability of discrimination on the y-axis. The green line shows objects that we identified as scrap, the red line indicated objects we identified as UXO. The dark blue circle represents “stop digging” point from our interpretation, the magenta circle shows the number of false positives if the probability would be 95%, and the cyan circle shows the number of false positives if the probability would be 100%. The gray shaded area indicates 95% confidence interval. The graph shows that we correctly discriminated all mortars (cyan and magenta circles) and had 26 false positives (dark blue circle), which is 17% of the total number of objects submitted for discrimination. In this case we performed slightly worse, possibly due to an increased variability in the ground response.

## **CONCLUSIONS**

The field survey at a former military site showed that a multiple-transmitter multiple-receiver system can accurately detect, locate, and characterize complex targets. Moreover, the system can clearly distinguish between symmetric intact UXO and irregular scrap metal, and can resolve the intrinsic polarizabilities of the target from

observations at a single position. The objects were identified by estimating the probability that an object was a single UXO based on a training data set of known targets. Priority dig lists were constructed based on these probabilities. The important outcome of this survey was that using our approach, we were able to identify all UXO and that even with the most conservative “stop digging” point we added only about 7%, and 17% respectively, of unnecessary digs (digging scrap) to the total number of excavation points in two different surveys.

A traditional procedure for UXO discrimination involves a detection survey, data post-processing and anomaly identification, as well as the surveying of identified anomaly locations, and reacquisition or a cued survey. We demonstrated a mode of operation that involves detection and characterization/discrimination at the same time, the advantage of which is that target reacquisition is not necessary for discrimination. Hence, at the expense of smaller daily coverage, this system eliminates surveying costs and a second, cued survey.

Ground response imposes an early time limit on the time window available for target discrimination. Once the target response falls below the ground response it will be poorly resolved, especially since the ground response itself is variable due to the inhomogeneous nature of the near surface. This might be the case for small or deep UXO in magnetic soils. We observed increased variability in the ground response in one area of the cued survey. This might have influenced the larger number of false positives in our priority dig list. However, since 4.2” mortars are relatively large it did not affect our UXO identification.

Our current approach works for isolated objects only. At the moment, in the case of non-UXO response, we are unable to discriminate a single piece of scrap from a combination of scrap and UXO. If multiple objects are present, a different approach is necessary and this is an area of future research.

This site contained two major classes of targets – UXO and scrap metal. The next step in our research is to apply an improved interpretation algorithm to a survey area where multiple munitions are present, and to discriminate those munitions from harmless scrap metal.

### **ACKNOWLEDGMENTS**

This research was supported by the Office of Management, Budget, and Evaluation of the U. S. Department of Energy under Contract No. DE-AC02-05CH11231 and the U. S. Department of Defense under the Environmental Security Technology Certification Program Project # MM-0437.

### **REFERENCES**

Baum, C. E., 1999, Low frequency near-field magnetic scattering from highly conducting, but not perfectly conducting bodies *in* C. E. Baum, ed., Detection and identification of visually obscured targets: Taylor & Francis, 163–217.

- Bell, T. H., B. J. Barrow, and J. T. Miller, 2001, Subsurface discrimination using electromagnetic induction sensors: *IEEE Transactions on Geoscience and Remote Sensing*, **39**, 1286–1293.
- Cazares, S., M. Tuley, and M. May, 2008, The UXO discrimination study at the former Camp Sibert: Institute for Defense Analyses Document D-3572.
- Gasperikova, E., J. T. Smith, H. F. Morrison, and A. Becker, 2006, UXO detection and characterization using new Berkeley UXO discriminator (BUD): AGU Joint Assembly.
- Gasperikova, E., J. T. Smith, H. F. Morrison, and A. Becker, 2007, Berkeley UXO discriminator (BUD): *SAGEEP Proceedings*, **20**, 1049–1055.
- Hoel, P. G., S. C. Port, and C. J. Stone, 1971, *Introduction to Probability Theory*: Houghton Mifflin Company.
- Huang, H., B. SanFilipo, A. Oren, and I. J. Won, 2007, Coaxial coil towed EMI sensor array for UXO detection and characterization: *Journal of Applied Geophysics*, **61**, 217–226.
- Geophysical prove-outs for munitions response projects, 2004, Technical and regulatory guideline: The Interstate Technology and Regulatory Council, <http://www.itrcweb.org/guidancedocument.asp?TID=19>, 79 p., accessed July 29, 2008.
- Khadr, N., B. J. Barrow, T. H. Bell, and H. H. Nelson, 1998, Target shape classification using electromagnetic induction sensor data: *Proceeding of the UXO Forum*, 8 p.
- McNeill, J. D., and M. Bosnar, 1996, Application of time domain electromagnetic techniques to UXO detection: *Proceeding of the UXO Forum*, 34-42.

- Pasion L. R., and D. W. Oldenburg, 2001, Locating and determining dimensionality of UXO's using time domain electromagnetic fields: *Journal of Environmental and Engineering Geophysics*, **6**, 91–102.
- Pasion, L. R., S. D. Billings, D. W. Oldenburg, and S. E. Walker, 2007, Application of a library based method to time domain electromagnetic data for the identification of unexploded ordnance: *Journal of Applied Geophysics*, **61**, 279–291.
- Report of the Defense Science Board Task Force on Unexploded Ordnance, 2003: Office of the Under Secretary of Defense for Acquisition, Technology, and Logistics, <http://www.acq.osd.mil/dsb/reports/uxo.pdf>, accessed July 29, 2008.
- Smith, J. T., and H. F. Morrison, 2004, Estimating equivalent dipole polarizabilities for the inductive response of isolated conductive bodies: *IEEE Transactions on Geoscience and Remote Sensing*, **42**, 1208-1214.
- Smith, J. T., and H. F. Morrison, 2005, Optimizing receiver configurations for resolution of equivalent dipole polarizabilities in situ: *IEEE Transactions on Geoscience and Remote Sensing*, **43**, 1490-1498.
- Smith, J. T., H. F. Morrison, L. R. Doolittle, and H-W. Tseng, 2007, Multi-transmitter null coupled systems for inductive detection and characterization of metallic objects: *Journal of Applied Geophysics*, **61**, 227–234.
- Snyder, D. D., and D. George, 2005, A dual-mode TEM and magnetics system for detection and classification of UXO: *SAGEEP Proceedings*, **18**, 1244–1253.
- Survey of Munitions Response Technologies, 2006: The Environmental Security Technology Certification Program, the Interstate Technology & Regulatory Council, and the Strategic Environmental Research and Development Program,

<http://www.itrcweb.org/guidancedocument.asp?TID=19>, 204 p., accessed July 29, 2008.

Won, I. J., D. A. Keiswetter, D. R. Hanson, E. Novikova, and T. M. Hall, 1997, GEM-3: A monostatic broadband electromagnetic induction sensor: *Journal of Environmental and Engineering Geophysics*, **2**, 53-64.

Wright, D., C. Moulton, T. Asch, P. Brown, M. Nabighian, Y. Li, and C. Oden, 2007, ALLTEM UXO detection sensitivity and inversions for target parameters from Yuma proving ground test data: *SAGEEP Proceedings*, **20**, 1422–1435.



## LIST OF FIGURES

**Figure 1.** (a) Instrument photo, (b) Schematic of transmitter and receiver positions.

**Figure 2.** Principal polarizability curves as a function of time for 4.2-inch mortar.

**Figure 3.** Principal polarizability curves as a function of time for a half-round (scrap metal).

**Figure 4.** Detection plot - a field value normalized by a background variation for a 4.2-inch mortar as a function of depth. Solid line indicates the response for a horizontal orientation of the 4.2-inch mortar (least favorable). Dashed line indicates the response for a vertical orientation of the 4.2-inch mortar (most favorable).

**Figure 5.** Principal polarizability curves as a function of time for a small scrap.

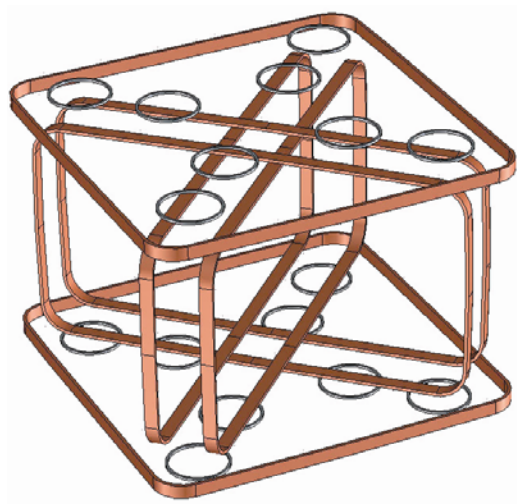
**Figure 6.** Principal polarizability curves as a function of time for a baseplate.

**Figure 7.** Detection map of the survey area.

**Figure 8.** (a) ROC curve for the survey area priority dig list, (b) ROC curve for the cued targets priority dig list.



(a)



(b)

**Figure 1.** (a) Instrument photo, (b) Schematic of transmitter and receiver positions.

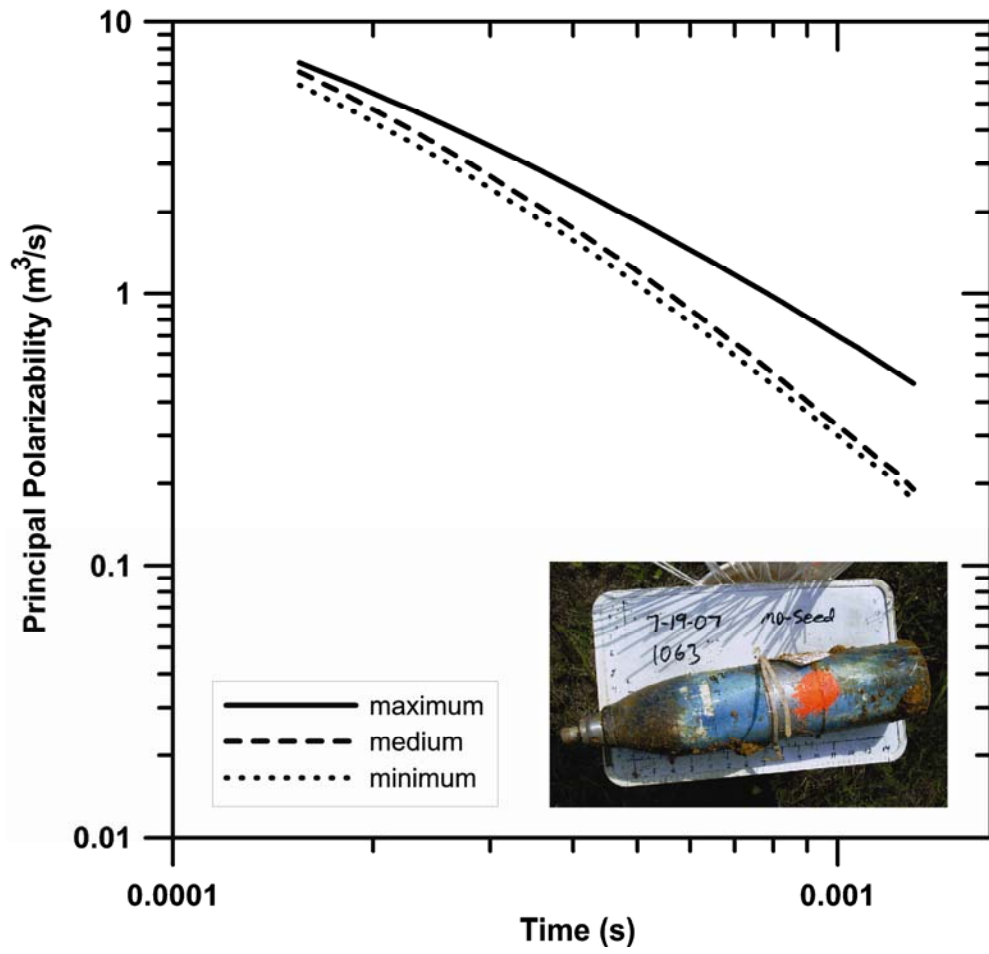
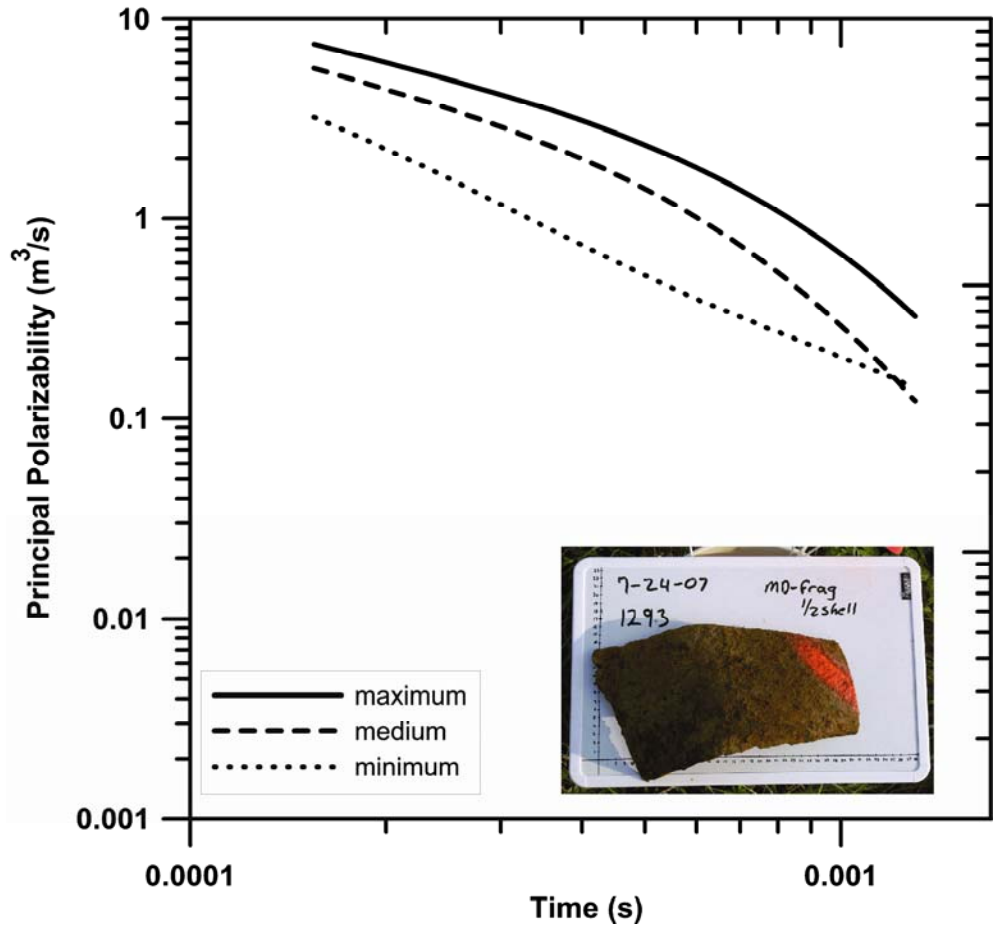
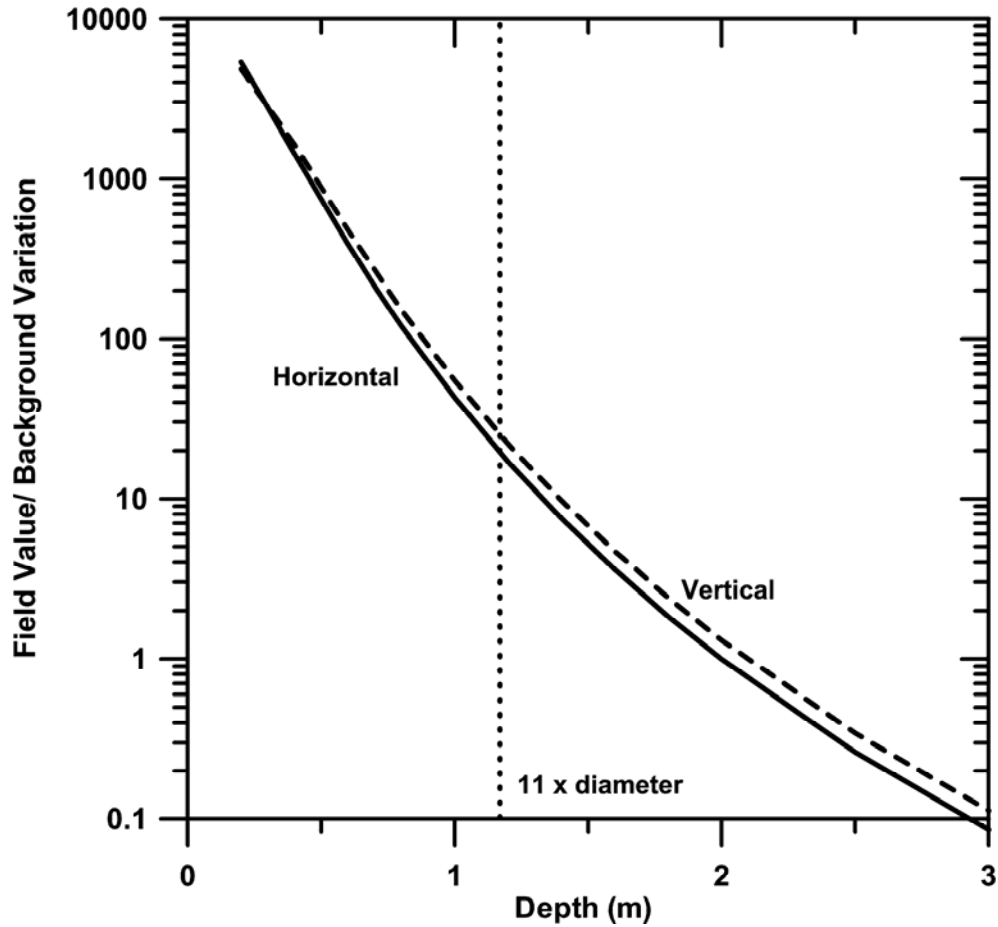


Figure 2. Principal polarizability curves as a function of time for 4.2-inch mortar.



**Figure 3.** Principal polarizability curves as a function of time for a half-round (scrap metal).



**Figure 4.** Detection plot - a field value normalized by a background variation for a 4.2-inch mortar as a function of depth. Solid line indicates the response for a horizontal orientation of the 4.2-inch mortar (least favorable). Dashed line indicates the response for a vertical orientation of the 4.2-inch mortar (most favorable).

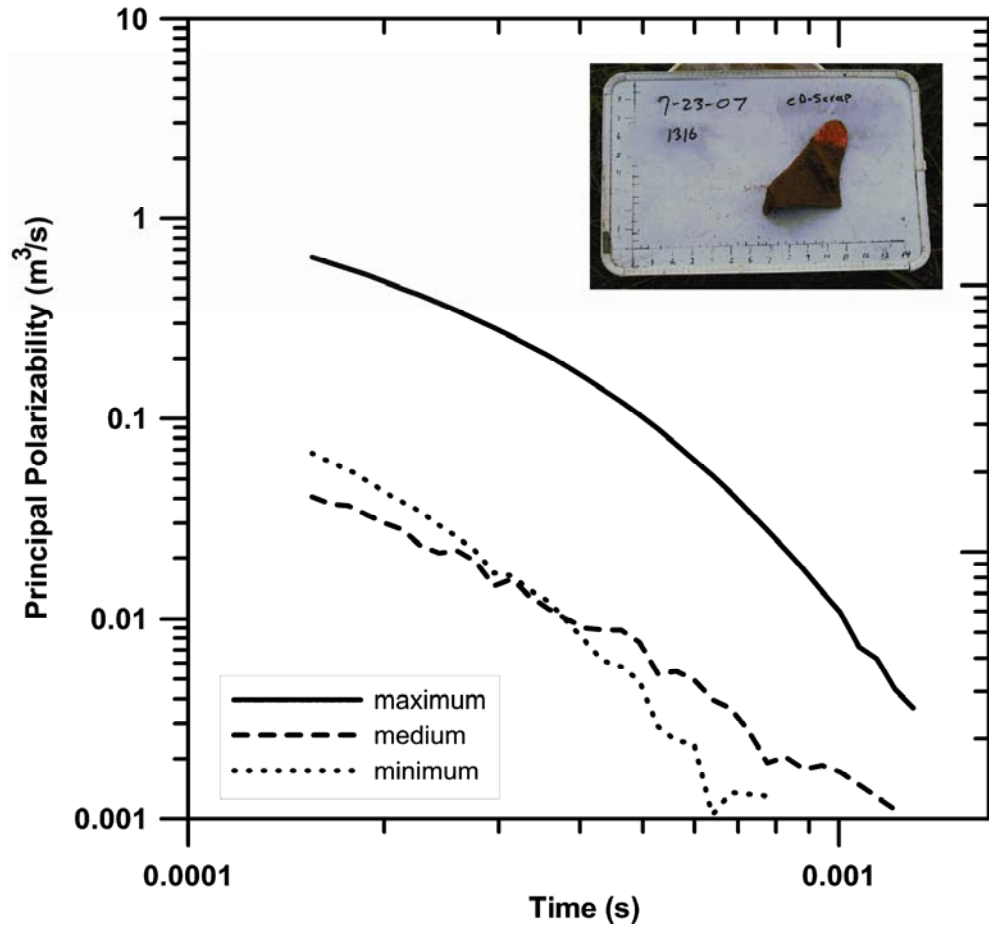


**Figure 5.** Principal polarizability curves as a function of time for a small scrap.

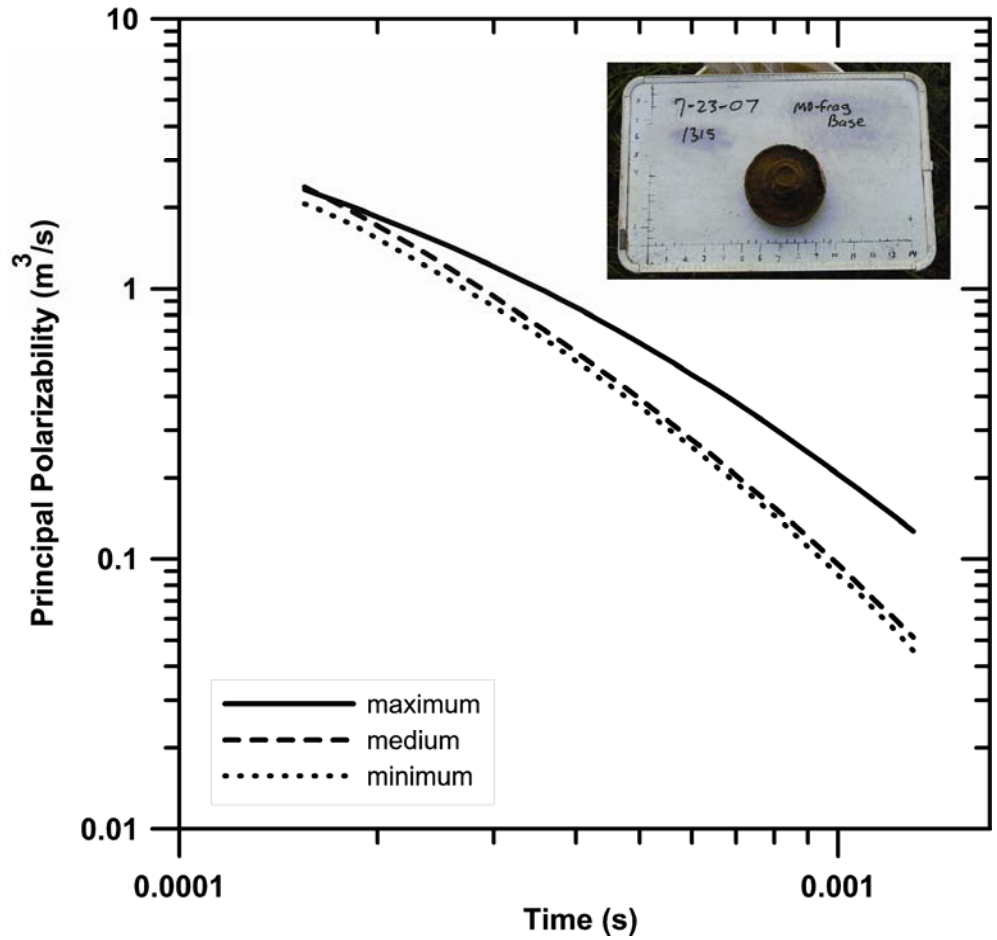


Figure 6. Principal polarizability curves as a function of time for a baseplate.

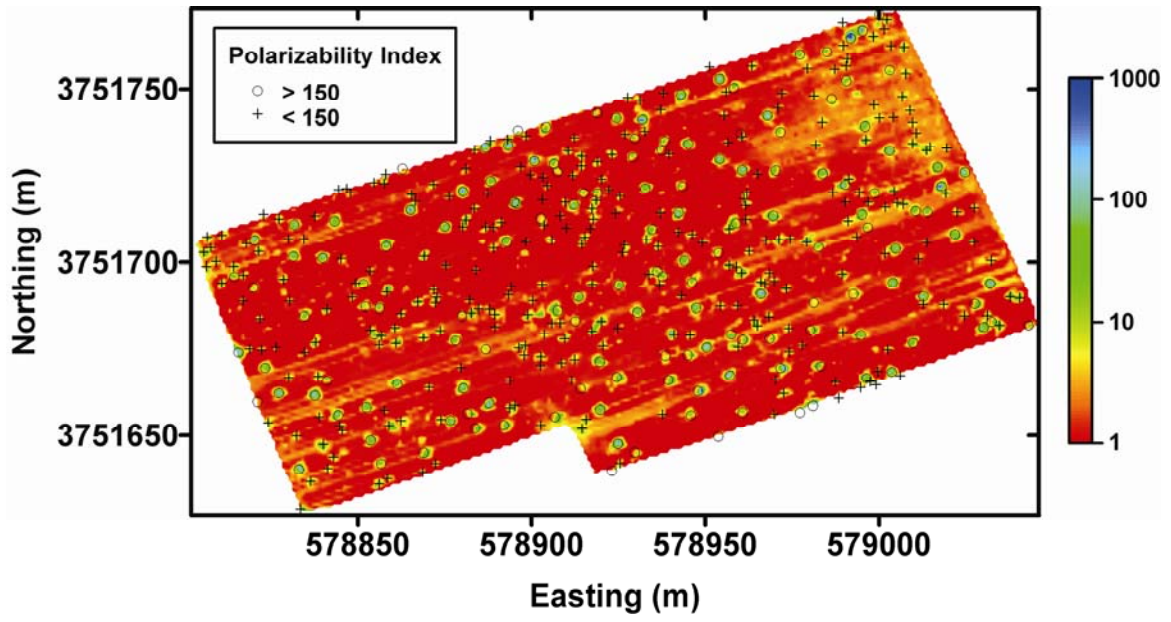
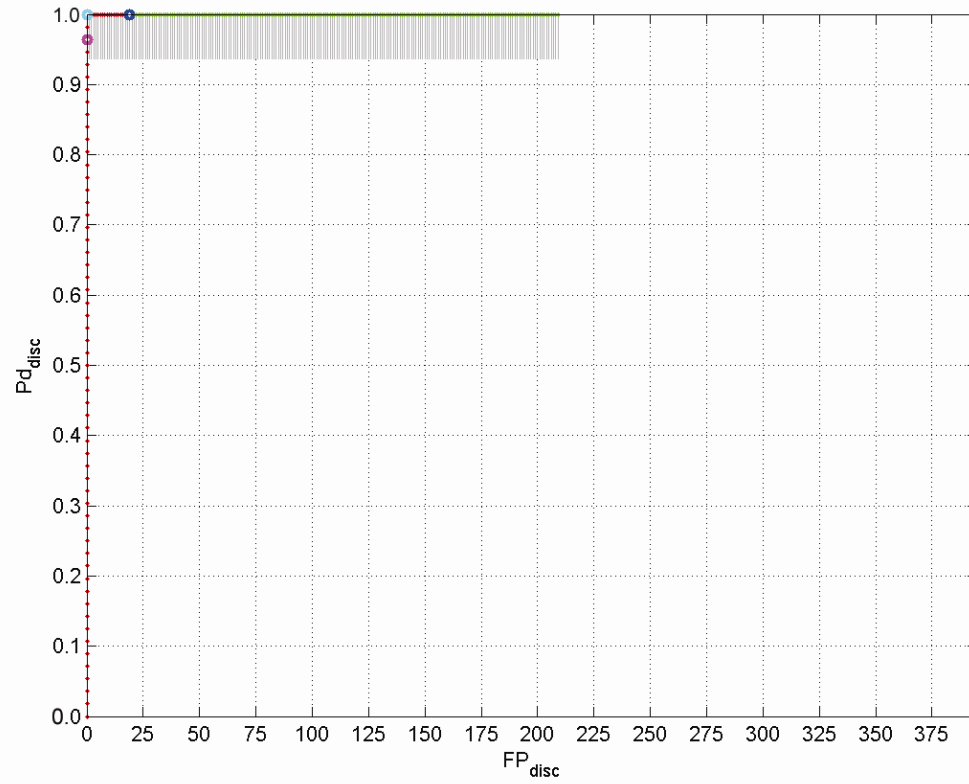
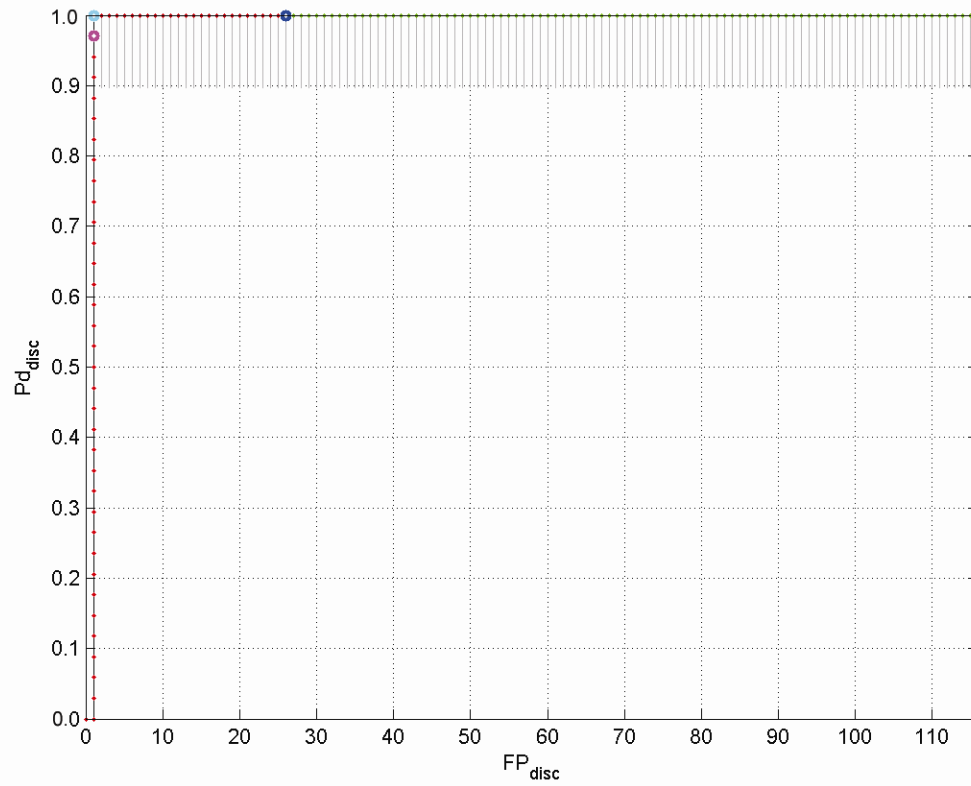


Figure 7. Detection map of the survey area.





(a)



(b)

**Figure 8.** (a) ROC curve for the survey area priority dig list, (b) ROC curve for the cued targets priority dig list.